

## Flood hazard mapping of the Welang river, Pasuruan, East Java, Indonesia

Entin Hidayah, Gusfan Halik, Indarto Indarto & Dian Wahyu Khaulan

To cite this article: Entin Hidayah, Gusfan Halik, Indarto Indarto & Dian Wahyu Khaulan (2022): Flood hazard mapping of the Welang river, Pasuruan, East Java, Indonesia, Journal of Applied Water Engineering and Research, DOI: [10.1080/23249676.2022.2114025](https://doi.org/10.1080/23249676.2022.2114025)

To link to this article: <https://doi.org/10.1080/23249676.2022.2114025>



Published online: 24 Aug 2022.



Submit your article to this journal [↗](#)




View related articles [↗](#)



View Crossmark data [↗](#)

## Flood hazard mapping of the Welang river, Pasuruan, East Java, Indonesia

Entin Hidayah <sup>a\*</sup>, Gusfan Halik <sup>a</sup>, Indarto Indarto <sup>b</sup> and Dian Wahyu Khaulan<sup>a</sup>

<sup>a</sup>Department of Civil Engineering, University of Jember, Jember, Indonesia; <sup>b</sup>Department of Agricultural Engineering, University of Jember, Jember, Indonesia

(Received 15 September 2021; accepted 13 August 2022)

The availability of a flood hazard map is beneficial during flood risk reduction. However, there is a lack of high-resolution topographic data, which is a map realization obstacle. Therefore, this study aims to construct flood hazard maps based on hazard levels for various flood return periods. The 2D-hydrodynamic from the Hydrologic Engineering Center's River Analysis System (HEC-RAS) and Digital Surface Models (DSM) from Unmanned Aerial Vehicle (UAV) imagery were used for generating inundation maps. The results showed that simulation of return periods for 2 and 10 years illustrated a 37% increase in flood hazard levels. Furthermore, there was an increased danger level for locations that were exposed to flood inundation. This occurred in housing, some roads, and rice fields. Ultimately, this study mitigates flood hazards through the determination of evacuation directions, urban spatial planning, and informed flood mitigation measures.

**Keywords:** Flood modeling; hydraulic models; unmanned aerial vehicle; two-dimensional models; velocity measurements; flood risk

### 1. Introduction

Flooding is a hazardous natural disaster that disrupts communication and transportation, harms lives, destroys materials, and severely compromises infrastructures. Climate change has affected rainfall patterns, leading to an increased rainfall frequency, intensity, and flooding probability (IPCC 2014; Rizzi et al. 2016). Furthermore, extreme weather has also affected flooding frequency in the Welang river 29 times from 2011 to 2016 (Sari et al. 2018). These floods threatened the plains of 6 villages and inundated the national road. Traffic jams on provincial highways, damaged infrastructures, and hampered economic and social activities are also other flood effects. Therefore, risk management such as damage estimation plays a vital role in flood reduction. The support of flood hazard management in a safe area requires detailed flood modeling (Peña and Nardi 2018).

Integrating remote sensing data in hydraulic models effectively supports decision-making and risk management in flood-prone areas (Vozinaki et al. 2017). High-resolution topographic data input is the main requirement for hydraulic modeling or detailed flood mapping to construct a flood hazard map for residential locations exposed to inundation risk (Peña and Nardi 2018; Petroselli et al. 2019). Various remote sensing data were used, such as 12-m WorldDEM, 30-m SRTM, 30-m ALOS, and 30-m ASTER DEMs show different resolutions of satellite

images have sensitivity to the depth and extent of flooding for hydraulic model simulations (Farooq et al. 2019). LiDAR can offer high-density and high-resolution DEM, resulting in higher flood modeling accuracy. However, the data's filtering process for DEM generation and point density is time-consuming in computing and simulating the flood model (Muhadi et al. 2020). Lack of high-resolution DEM, and limited funding and time are problems in flood inundation modeling. The DSM from UAV image provides very high resolution and accurate DEM at low survey costs and time (Akturk and Altunel 2019; Annis et al. 2020; Martínez-Carricondo et al. 2018). Furthermore, DSM processing for drainage network extraction was subject to errors and potential uncertainty (Nardi et al. 2019). These essentially need to be minimized by providing DSM maps as input for hydraulic modeling through corrected UAV imagery.

Flood mapping using a hydraulic model (HEC-RAS) adequately and effectively maps inundation to assess future flood risk in riverbank areas (Aryal et al. 2020; Mourato et al. 2017; Shustikova et al. 2019). besides that, The HEC-RAS models can be calibrated against discharge or inundated area data and give good predictions of inundated area, The predictive power of the models calibrated against inundation extent or discharge for one event can thus be measured using independent validation data for the second (Horritt and Bates 2002). This hydraulic 1D

\*Corresponding author. Email: Entin Hidayah [entin.teknik@unej.ac.id](mailto:entin.teknik@unej.ac.id) Department of Civil Engineering, University of Jember, St. Kalimantan No. 37Jember, Indonesia

model estimates flood inundation only for a simple grid system (Vojtek et al. 2019). Meanwhile, for complex network systems, 2D models are more adequate (Shustikova et al. 2019; Vojtek et al. 2019). To overcome the lack of high-resolution rain data in flood mapping, these complex systems use the HEC-RAS 2D flood model with DSM input from UAV images which showed significant results (Yalcin 2019). The HEC-RAS modeling is effective based on the match between the UAV image resolution and its mesh resolution and accurately depicts depth by simulating various mesh resolutions (Shustikova et al. 2019). For a 2D HEC-RAS hydrodynamic modeling process, a resolution match between the Digital Elevation Model DEM and the mesh is required to obtain optimal accuracy (Ongdas et al. 2020; Shustikova et al. 2019).

Therefore, this study aims to solve problems of hydraulic modeling and the lack and uncertainty of spatial data affecting flood hazard mapping accuracy in the Welang river. DSM data was generated from UAV images and used for high-resolution data provisioning to support shortages. Furthermore, flood simulation to obtain modeling accuracy uses HEC-RAS 2D through the application of a non-steady flow calibrated with historical observation data of flood events in the field. Mesh elements which lead to spatial error are generally square and uniform. These elements have the disadvantage of same-sized shapes throughout the meshes and an increased mesh size requirement to reduce uncertainty. This study tries various mesh sizes with or without break lines to improve model performance. Furthermore, 2D model simulations for 2 and 10 years return periods describe flood hazard levels.

## 2. Methodology

### 2.1. Study area

This study was carried out in the downstream area of the Welang watershed, East Java, Indonesia, as shown in Figure 1. This area was 3.31km<sup>2</sup> and included five villages that were prone to flooding, namely Kraton, Tambakrejo, Karangketuk, Sukorejo, and Randusari villages. Its upper and lower limit or outlet was the Sukorejo village and railroad bridge, respectively. Furthermore, it was also crossed by an arterial road connecting the Java island to Bali. Floods along the Welang River inundated thousands of homes and led to a lengthy traffic spike. Currents were measured at the AWLR Dhompo station, located 4.5 km from Kraton village.

### 2.2. Procedure

Three steps were carried out, namely, (1) preparing 3D maps, (2) inundations modeling in HEC-RAS, and (3) construction of the flood hazard maps shown in Figure 2. As for the first step, the following activities were carried out:

collection of Ground Control points GCPs, followed by orthophoto mosaic calibration using GCPs data to obtain the smallest square error, and DSM processing and validating. For the second step, the following activities were carried out, (1) modifying the terrain data with a RAS Mapper and validating the modified data, and (2) modeling the flood hazards in the 2D hydrodynamic model analysis. The third step involved flood hydrographs simulation using 2, 10, and 20-year return periods.

### 2.3. Preparation of 3D-Maps

The GCPs were obtained by adjusting the coordinate points in the Global Positioning System. These points (GCPs) were placed on visible features and distributed around the study area shown in Figure 3. Furthermore, measurements were carried out in World Geodetic System WGS 84 datum and Universal Transverse Mercator UTM zone 49S projection. The L1 single frequency geodetic GPS and a Da-Jiang Innovations DJI Phantom 3 UAV drone with a 12.4 MP camera at a flying height setting of 12 m from the ground with overlap and side lap values of 80% and 70%, respectively, were used during the study. This UAV took 738 images, which were then processed and analyzed using image processing software.

A DSM construction is based on elevation points in the weighted cloud using the Natural Neighbour interpolation method. This obtained results, were 3D surface models (DSM) with resolution output of 12-cm x 12-cm and an orthophoto mosaic (5-cm). The DSM and mosaics were exported as Geo TIFF inputs in HEC-RAS. Furthermore, DSM accuracy was measured by comparing its coordinate points and those of 20 other GCPs. According to the National Standard for Spatial Data Accuracy NSSDA (Federal Geographical Data Committee 1998), the precision check for x and y points should be measured based on a confidence level of 95%. The accuracy values for the horizontal direction were equal to 1.7308 multiplied by the Relative Root Mean Square Error RMSEr values in this direction. It was assumed in this equation that RMSE<sub>x</sub> was equal to RMSE<sub>y</sub>, and the error is normally distributed and independent in each of the x- and y-components. Meanwhile, the accuracy values for the vertical direction were equal to 1.96 multiplied by RMSE<sub>z</sub> values in the vertical direction.

### 2.4. Inundation modeling in HEC-RAS

Hydrologic Engineering Centre (A.C.E. 2010) HEC-RAS is a free software enabling users to carry out various hydraulic simulations on river flow. It was widely used and is an efficient program for developing food models and inundation maps. HEC-RAS can also be applied for steady and unsteady flows (Demir and Kisi 2016; Yalcin 2019).

The first modeling step was the modification of a terrain raster for the study area. This modified raster was

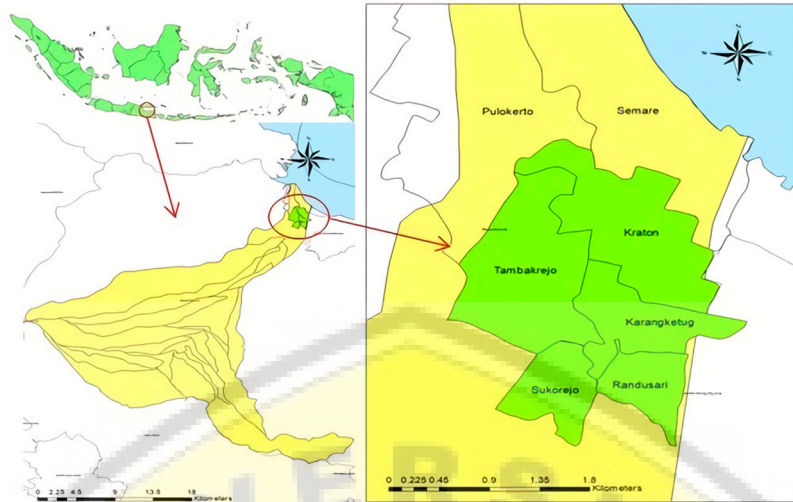


Figure 1. Study of Area.

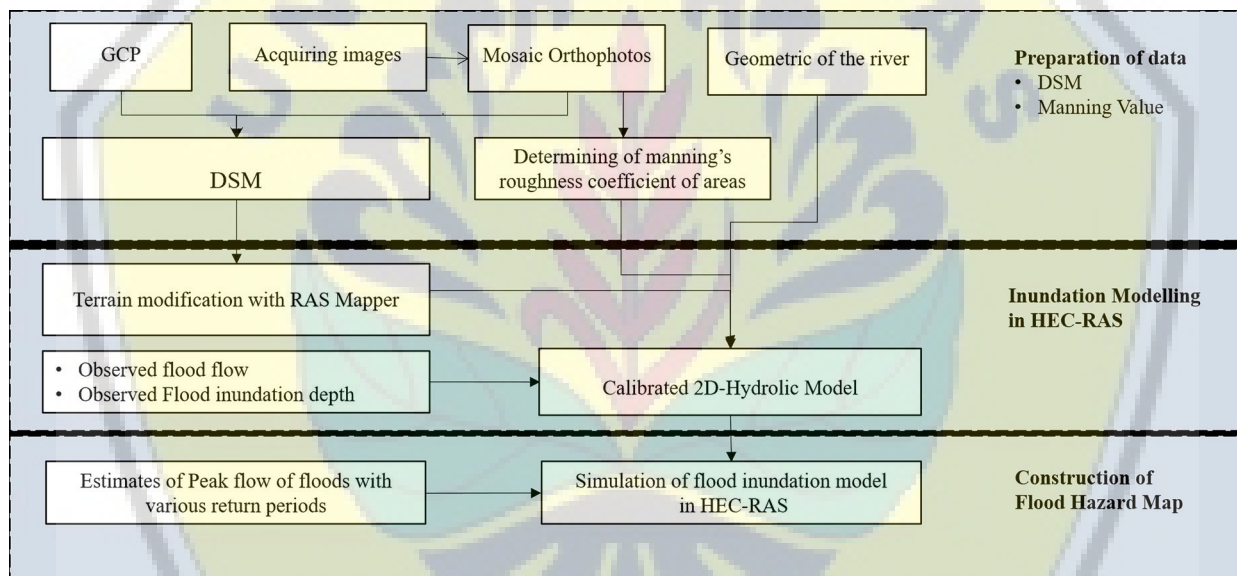


Figure 2. The Steps in Mapping Flood Hazard.

set as the input for a RAS Mapper interface. Furthermore, polygons of 2D flow areas representing flood zone borders were plotted as terrain models in the geometric data editor software. A 2D computational mesh was created with grid sizes of 5, 10, and 20 m. After the mesh was constructed, upstream and downstream boundary lines were set in the 2D flow areas. Features of these flow areas were set (shown in Figure 4), and mesh computing was carried out to develop a hydraulic property table.

The result of the 2D geometrical process in RAS Mapper was a graph showing the relationship between elevation and mesh volume. Relationships between hydraulic properties, such as elevation versus area, wetted perimeter, and roughness, were also shown. A hydraulic property table was used to control water movement into, through, and

away from the mesh. The 2D unsteady flow setting was used for this inundation modeling. Furthermore, HEC-RAS can route an unsteady flood by employing the Saint-Venant full momentum or diffusion wave equations (Yalcin 2019). In this study, the diffusion wave equation was selected for use. Equation (1) below expresses unsteady flow with uniform density and hydrostatic pressure for 2D diffusive waves.

$$\frac{\partial H}{\partial t} + \frac{\partial(hu)}{\partial x} + \frac{d(hv)}{dy} + q = 0 \quad (1)$$

where  $t$  (s) is time,  $H$  (m) is the water level elevation,  $h$  (m) is the water depth,  $u$  and  $v$  (m/s) are the velocity components in the  $x$  and  $y$  directions, respectively, and  $q$  (m/s) is the inflow.

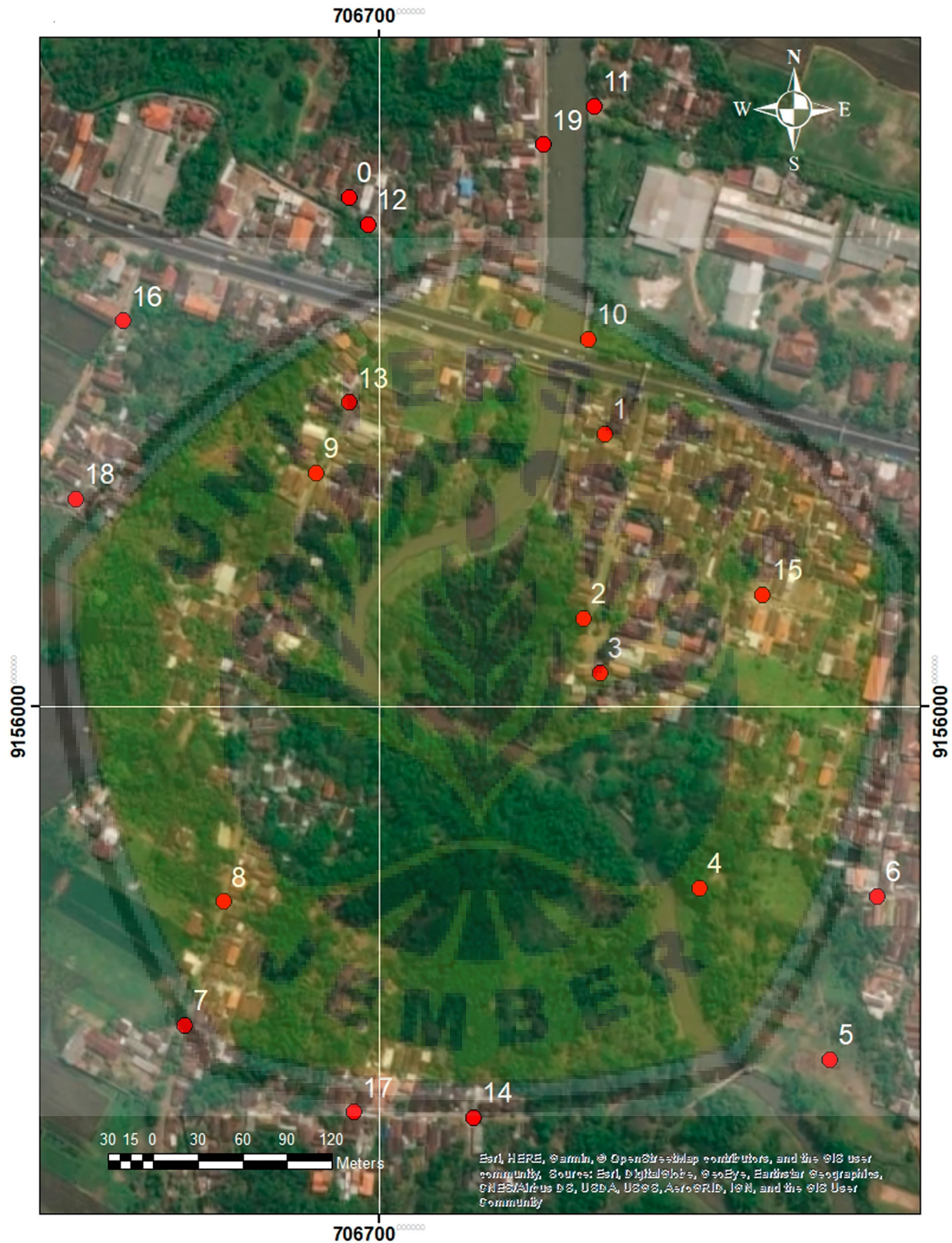


Figure 3. The GCP's Distribution in The Area of Study.



Figure 4. Geometric Data Representation in HEC-RAS 5.0.

In this 2D modeling, two boundary conditions were set using unsteady flow. The energy slope was set at 0.036 m/m, and it was assumed that the region near the river's upstream boundary condition had this same energy value. Furthermore, the standard depth was used in the downstream boundary conditions, while the friction slope required for boundary conditions was set to 0.010 m/m. Manning roughness coefficients for each land use in the 2D flow area were classified into three land cover types identified manually from the orthophoto maps. The Manning coefficient table was used as the reference in assigning coefficient values to the land covers. These coefficients are manually represented as polygon lines on orthophotos in the data menu region of a Geometric Editor software.

### 2.5. Performance of hydraulic model

Flood inundation can be calibrated by cross-checking the model depth against the actual flood depth measured at several points in the field (Akturk and Altunel 2019). Model performance is calculated based on the smallest error value from the water depth between the hydraulic simulation results and observations of field floods. Furthermore, the process of obtaining this error is carried out through the calibration of an inundation model at 5 flood locations. The best model performance can be achieved by adjusting the roughness value and trying grid meshes with or without break lines (Ongdas et al. 2020). For this study, three different grid sizes simulated the same event. On January 5, 2017, hourly flood flow data in Welang River was used for calibration for two days.

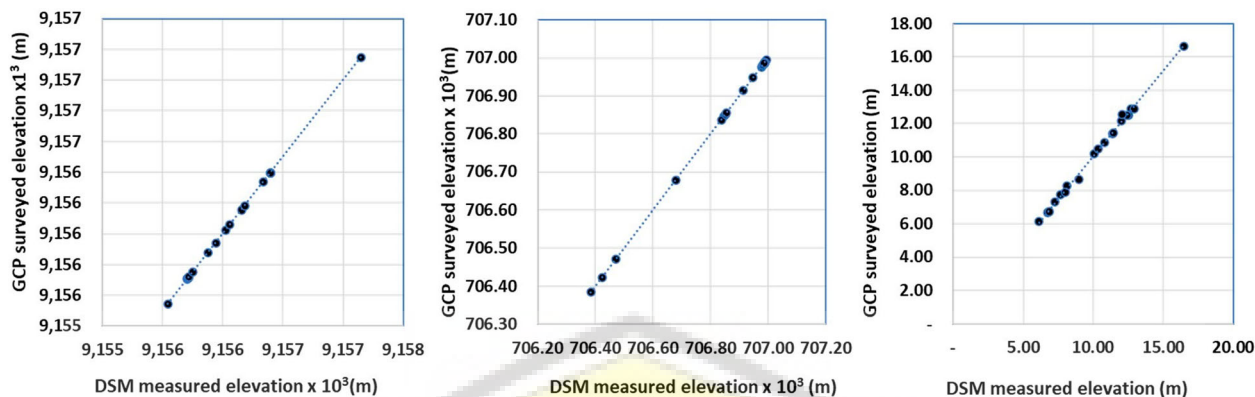


Figure 5. Graph of The Relationship Between GCP and Model Values at X, Y, and Z Coordinates.

## 2.6. Prediction of flows and level of flood hazard

After the model parameters were set, flood simulation was carried out through the use of designed flood flows. In modeling the flood hydrograph in the Welang River, (Febriyanto et al. 2018), the transformation method and SCS curve number were both used. The calibration results obtained a NASH effectiveness of 0.873. Furthermore, the modeling used two different direct runoff methods in which the Snyder's Unit Hydrograph was the most reliable calibration model, with a Nash value of 0.935 on January 5, 2017. The flow estimates were based on return periods of 2 and 10 years, representing a recurring flood event at Welang river. Peak flows in model simulations for this 2-year and 10-year return periods were 104.1 and 149.8  $\text{m}^3/\text{s}$ , respectively. The simulation duration was set to 8 h for all flood scenarios according to the base time of the hydrograph (Sugiantara 2020).

The level of flood hazard was assessed based on the depth and speed of inundation. Also, hazard levels can be based on depth which is divided into three, namely, low ( $<0.76$  m), medium (0.76-1.5 m), and high ( $>1.5$  m). Meanwhile, the hazard levels based on flow velocity are divided into low ( $<0.05$  m/s), medium (0.05-0.1 m/s), and high ( $>0.1$  m/s).

## 3. Result

### 3.1. Accuracy of DSM

A UAV image with a size of  $13 \times 13$  cm was used as input for hydrodynamic modeling. Figure 5 shows the error measurements of 20 points calculated from the difference between the GCP and model values at the x, y, and z axes. Furthermore, error values were Gaussian distributed based on Anderson Darling's goodness of fit test with 95% confidence. The results shown in Figure 5 are the RMSE values for horizontal (r) and vertical directions (z), which were 0.667 and 0.161 m, respectively. Horizontal accuracy per NSSDA was 1.155 m, and the vertical accuracy was 0.316 m as per the American Society for Photogrammetry and Remote Sensing ASPRS.

Based on the NSSDA accuracy, the horizontal RMSE x, and y values in this study were categorized in class 1 with a scale of 1: 5000. Furthermore, the vertical RMSE z value, according to the ASPRS accuracy standard, was classified as class 1 on the scale from 1: 5000 (FGDC (Federal Geographic Data Committee), 1998). The accuracy of this result was suitable for planning.

### 3.2. Calibration of 2D flood inundation modeling

The flood inundation in Welang River was estimated by 2D hydraulic modeling developed in HEC-RAS 5.0 using unsteady flow simulation. The model inputs were DSM maps, river geometry data, and flow data. Furthermore, the best model performance was obtained by trial and error calibration on manning values and improving mesh sizes. 2D flood inundation modeling is calibrated by cross-checking the simulation inundation depths against historical flood depths. The peak flood flow used in model calibration was 23  $\text{m}^3/\text{s}$ , with a simulation duration of three days. Calibration is carried out based on the history of flood inundation depth at three coordinate points in the residential areas of Tambakrejo village (1 location point) and Karangketug (2 location points), as shown in Table 1 and Figure 6. The mean relative error of the calibration results at the three points was 9%.

Improved mesh size used various sizes of 5m x 5m, 10m x 10m, and 20m x 20m with and without break lines are shown in Figure 7. Therefore, the results show that the larger the mesh size, the better the RMSE value. Break line addition on all sizes obtains a better performance impact than those obtained without it. Furthermore, the model bias value for all mesh sizes shows a negative value, which indicates model under-estimation. RMSE for mesh sizes of 5m x 5m are in the satisfactory category, while the 10m x 10m and 20m x 20m sizes are in the unsatisfactory and outstanding category, respectively.

The acceptable model calibration results through trial by error of manning based on land use, including settlements, paddy fields, and plantations, were 0.15, 0.025, and



Figure 6. Calibration of Flood Inundation Depth.

Table 1. Validation of flood inundation depth.

Point	Coordinate Points	Historical inundation depth (m)	Model inundation depth (m)	Absolute error (cm)	Relative error
1	706844.268, 9156402.984	1	1.25	25	4%
2	706680.156, 9156340.166	2	1.75	25	13%
3	706837.176, 9156058.136	1	1.10	10	10%

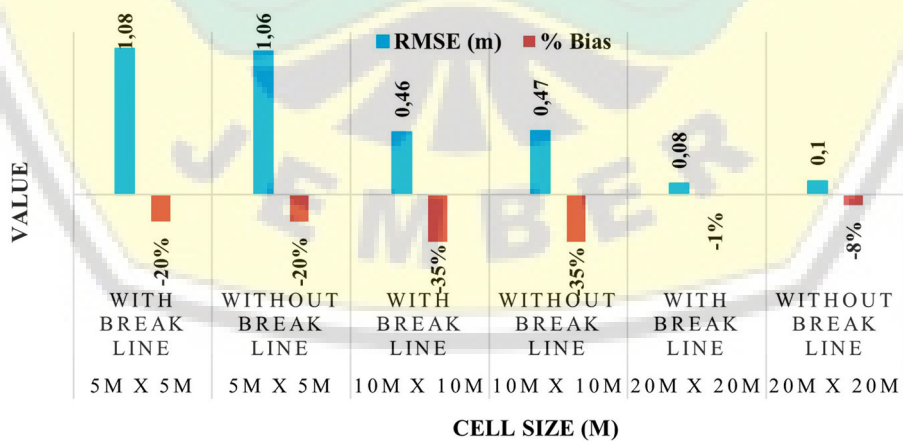


Figure 7. Measurement of historical flood inundation depths at three locations.

0.04, respectively, while the mesh size was 20m x 20m with a break line. Furthermore, the model's performance shows a perfect relationship with an RMSE value of 0.08 m and a Pbias of -1%, which was slightly underestimated.

The advantage of extending this mesh size is that it requires a shorter time in the modeling process. Referring to a previous study using HEC-RAS in Secchia River, improved mesh size was best at 100 m from three resolutions of 25,



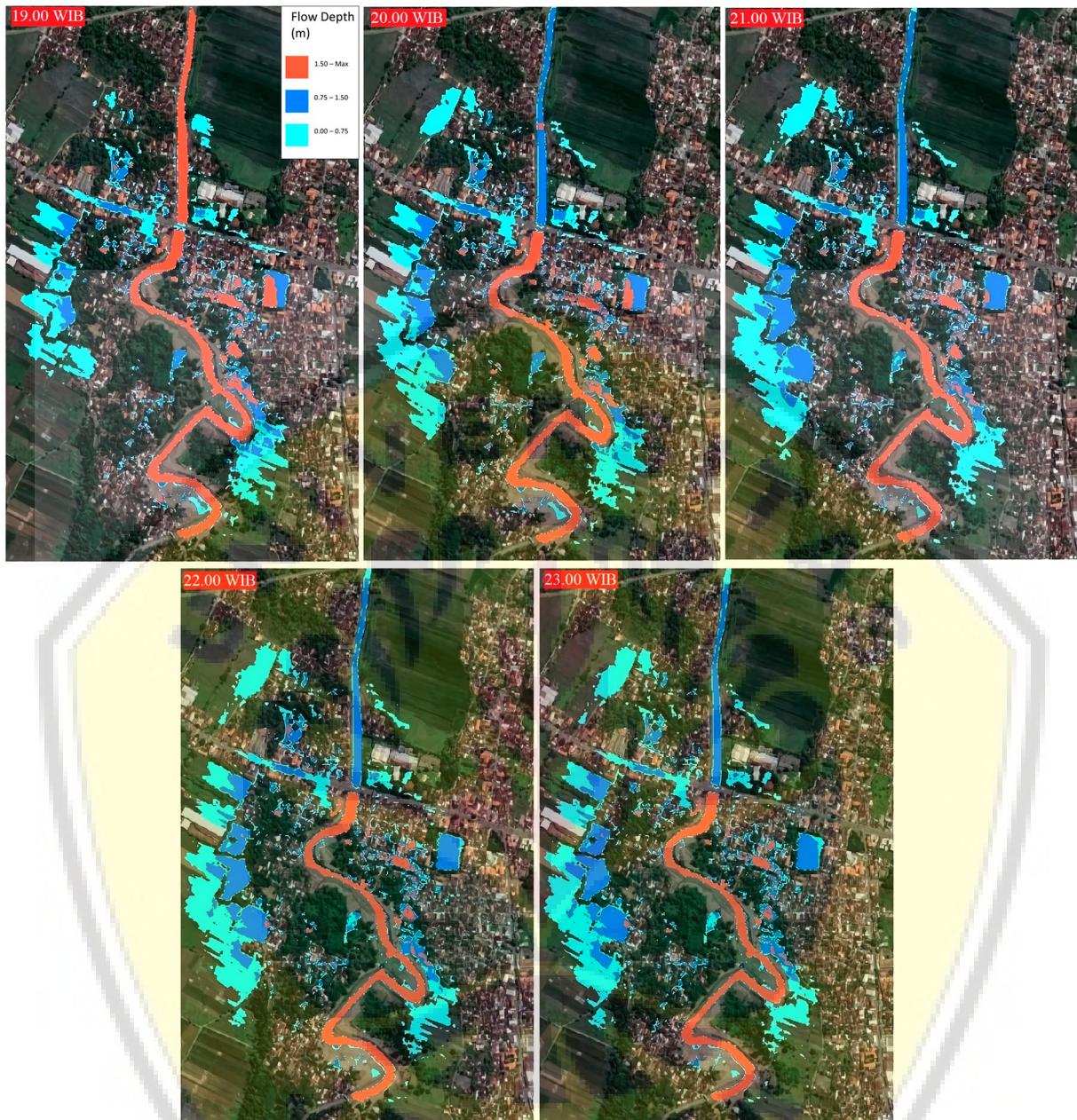


Figure 8. Changes In Flood Flow Depth (m) for 5 h from Model Calibration Results.

50, and 100 m with an accuracy rate of 0.84%. A greater depth of mesh size requires less time during the modeling process (Shustikova et al. 2019). Furthermore, in mapping flood hazards in the Yesil (Ishim) River in Kazakhstan, the best mesh resolution was at 25 m from the three resolution options, namely 25, 50, and 75 m, using break lines as modeling inputs (Ongdas et al. 2020). This study's results align with previous studies possessing a 13 cm resolution and an improvised mesh of 20 m using break lines as a mapping flood hazard reference.

The calibration analysis results of 2D flood inundation modeling in Figure 8 through RAS-Mapper present

the depth propagation patterns of flood flow over the floodplain for 5 h.

Based on RAS Mapper's Animator, the maximum flood inundation area reached 299,941 m<sup>2</sup> and occurred on January 5, 2017, between 19.00-23.00 Western Indonesian Time WIB. At 19.00 WIB flood levels along the river and Karangketug village was above 1.5 m, and the flood overflow occurred in 5 villages (Randusari, Karangketug, Sungiwetan, Tambakrejo, and Kraton). At 20.00-23.00 WIB, the flood depth's propagation pattern was the same for the downstream part of the river. Meanwhile, this depth decreased after the bridge. The flood area to the west of the

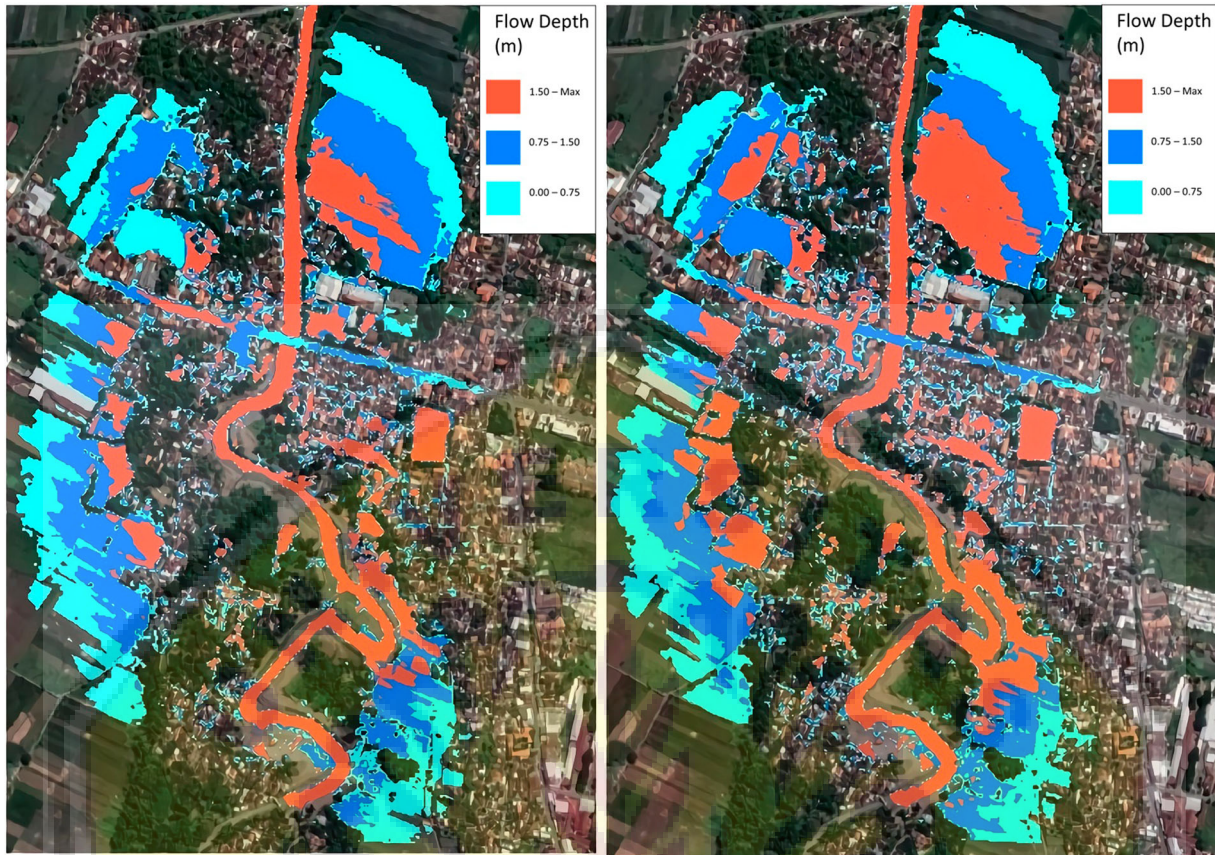


Figure 9. The Depth (m) of The Flood Inundation For 2-Year (a), and 10-Year (b) Return Periods.

river (Sungiwetan and Tambakrejo villages) increased and was accompanied by a reduction in depth. Meanwhile, the area east of the river did not increase and was accompanied by a depth increase.

This flood depth propagation pattern occurs due to bridge narrowing and shallow river elevation. Furthermore, the elevation in the area to the east of the river was lower than to the left. Therefore, based on field investigations, the calibration results show that this flood inundation propagation pattern is consistent with the incident history agreed by the community.

### 3.3. Prediction of the 2D flood hazard model

Prediction of flood hazard zones is consistent with the spatial distribution of regions in the six villages, including inundated housing areas, paddy fields, and plantation fields. In all 2 and 10 years return period scenarios, the capacity of Welang River was insufficient to carry the floodwaters downstream. It is, therefore, probable that future floodwater will inundate the riverbanks.

The Flood hazard prediction results in HEC-RAS were shown using two parameters of hazard levels, namely inundation depth and velocity. Furthermore, the flood hazard map results in Figure 9 showed that the river's capacity

could not accommodate the discharge for hazard level area locations of inundation depth between a 2 and 10 years return period. The flood hazard zone prediction in Figure 8 also includes six villages (Tambakrejo, Kraton, Karangketug, Randusari, Sukorejo, and Sungiwetan) used for residential areas, rice fields and plantation areas that are inundated by land. The Welang River is unable to drain floodwater downstream. Therefore, it is highly probable that future floods will inundate riverbanks, as shown in Figure 9. In general, the level of flood hazards on bridges and roads is lower than in settlements. This is due to its low positioning when compared to highways.

Furthermore, all village settlements were included in the category of high flood hazard levels except for those in the Randusari village, with moderate and low flood levels. As for rice fields and gardens, the level of flood hazard exists at all levels, while a high level of danger occurs in locations near rivers. Therefore, these results guide the community and government in a future with dangerous areas.

Figure 10 shows an overview of the area distribution for the 2 and 10 years flood return period. The total area for the 2-year return period was 563,302 m<sup>2</sup>, with area percentage details for low, medium, and high hazard levels as 199,849 m<sup>2</sup> (35.48%), 176,645 m<sup>2</sup> (31.36%), and 186,807 m<sup>2</sup>

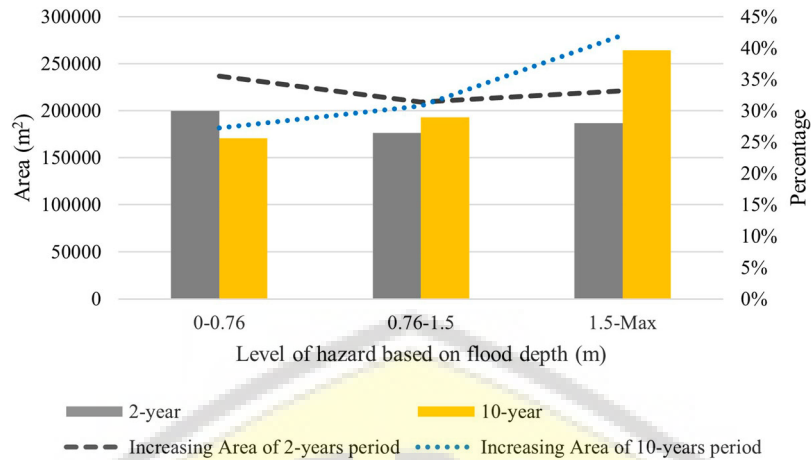


Figure 10. Graph of The Depth of Inundation at Each Level of Flood Hazard.

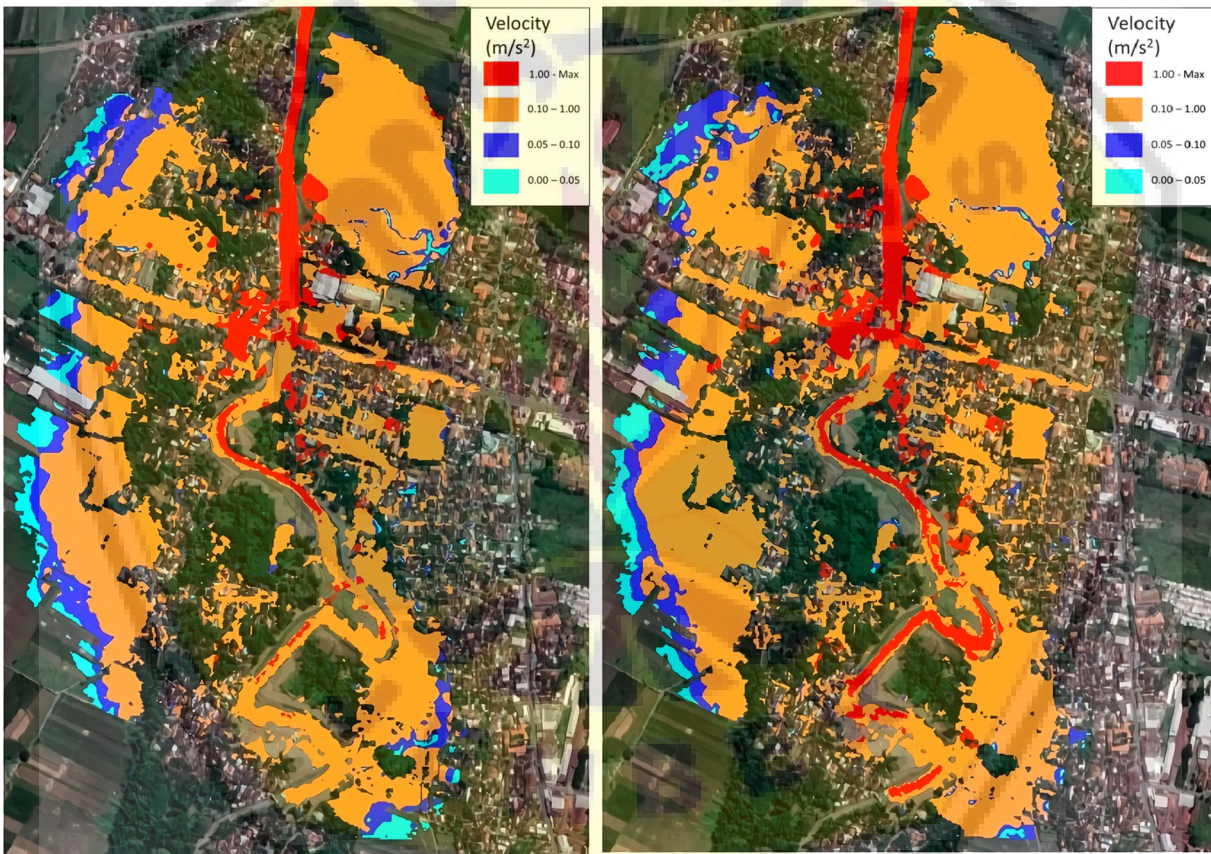


Figure 11. The velocity in 2-year and 10-year return periods scenarios.

(33.16%) respectively. Meanwhile, for the 10-year return period, the total location area was 628,133 m<sup>2</sup>, with area percentage details, for low, medium, and high hazard levels as 170,853 m<sup>2</sup> (27.20%), 193,206 m<sup>2</sup> (30.76%), and 264,073 m<sup>2</sup> (42.04%) respectively. The general inundation area extension from the 2-year to 10-year return period increased by 10.32%. However, this extension varies for different flood hazard levels from the return period. For

example, a high category flood hazard shows an increase in inundation area of 8.88%. Flood return periods are directly proportional to hazard levels, this is indicated by shallow river elevation and a concave right and left river area.

Based on the flow velocity level (Figure 11) for the 2 and 10-year return periods, almost all areas with high, and very high levels of flood susceptibility are located on river banks, borders, and around bridges. The flow rate is

very high for these two return periods, directly proportional to the flood discharge. However, the flow rate increases after the narrowing of the bridge. Therefore, the factors that affect the flow velocity here are an increase in flood discharge and a decrease in river capacity.

In the 2 and 10-year return periods, almost all areas showing a high hazard level and a very high category of flood vulnerability were located in the river area and around the bridge. Figure 11 shows the location of the flow velocity levels with these return periods. The very high flow velocity level for these two return periods was directly proportional to flood discharge; however, the speed level increased after the bridge narrowed.

The results of DSM accuracy, calibration, and hydraulic model simulation analysis can be explained as follows. DSM modeling uses a simple UAV imagery tool that obtains less than optimal results. To make up for this shortcoming, this 2D DSM hydraulic model yield can be improved by extending the mesh size to improve the performance. Furthermore, the simulation results of flood movement patterns, especially the identification of inundation depth, magnitude of speed, and flood arrival time in this study, determine the direction of structural and non-structural mitigation. The focus of structural mitigation is carried out by strengthening embankments at locations adjacent to settlements for the reduction of flood exposure, normalization of rivers, and widening of bridges. However, further studies are needed to consider natural-based solutions for this structural action. Therefore, the results of this study can be used as a reference for non-structural mitigation such as proper evacuation directions, spatial planning, early warning systems, and determination of rice fields that should be insured.

#### 4. Conclusions

The 2D hydrodynamic model with DSM input (based on UAV imagery) can produce high-resolution flood inundation maps. This approach provided a solution to overcome the lack of high-resolution data for DEM. The hydraulic model's accuracy is obtained through calibration based on the comparison of flood height from the simulation model with field observation data by adjusting the value of floodplain and channel friction. The calibration results using 2017 flood data can describe the actual field conditions with an average relative error of 9%. Simulation of various mesh sizes (5, 10, and 20 m) by including break lines improved the model's consistent performance, resulting in an outstanding RMSE value (0.08).

Flood scenarios using hydrographs with a return period of 2 and 10 years identify flood inundation depth, velocity, and arrival time. This answers factual questions about the threat of flood hazards at the local level. Furthermore, flood hazard maps are the basis for creating vulnerability maps to identify different types of land use, settlements,

and infrastructure as the first step toward comprehensive flood risk mapping.

Depth, flow velocity, and direction are also used to determine the direction of flood evacuation.

#### Acknowledgments

This study was funded by the Indonesian Ministry of Research, Technology, and Higher Education in 2020 through Graduate Study Grants. Significant data was provided by the Technical Implementation Unit of the Water Resource Management Agency (UPT PSDA) of Pasuruan Regency, Jawa Timur Province, Indonesia.

#### Disclosure statement

No potential conflict of interest was reported by the author(s).

#### Notes on contributors

**Entin Hidayah** Got his Bachelor Degree in civil engineering from Institut Teknologi Sepuluh Nopember Surabaya, Indonesia (1992), and has a Master of Urban Management (University of Canberra, Indonesia (2001). She has Doctoral in Civil Engineering (Institut Teknologi Sepuluh Nopember Surabaya, Indonesia (2011). She is working as a researcher and teacher at the University of Jember, Indonesia. Her areas of expertise include hydrology and hydraulic modeling, water resources management, and flood risk management.

**Gusfan Halik** Got his Bachelor Degree in water resources engineering from University of Brawijaya (UB), Malang – Indonesia (1995), and has a Master Degree in Civil Engineering (Institut Teknologi Sepuluh Nopember Surabaya, Indonesia (2002). He got Doctoral Degree in Civil Engineering from (Institut Teknologi Sepuluh Nopember Surabaya, Indonesia 2016). He is working as researcher and teacher at Faculty of Civil Engineering of Jember, East Java, Indonesia (since 1999). Her areas of expertise include hydrology modeling, climate change and data driven modeling.

**Indarto Indarto** Got his Bachelor Degree in Agricultural Engineering from Gadjah Mada University (UGM), Yogyakarta – Indonesia (1995), and has a DEA in Water Science from University of Montpellier (USTL- Univerisite Science et Technique de Languedoc) in 1998. He got a Doctoral Degree from the ENGREF de Paris in 2002. He is working as a researcher at University of Jember, East Java, Indonesia (since 1995). His areas of expertise include hydrological modeling, application of GIS and RS in the area of agriculture and water resources management.

**Dian Wahyu Khaulan** Got his Bachelor Degree in Civil Engineering from University of Jember (UNEJ), Jember – Indonesia (2017), and has a Master Degree in Civil Engineering from the same University (2020). He is working as researcher Civil Engineering at Faculty of University of Jember, East Java, Indonesia (since 2020).

#### ORCID

*Entin Hidayah*  <http://orcid.org/0000-0002-1233-6850>

*Gusfan Halik*  <http://orcid.org/0000-0002-5447-1268>

*Indarto Indarto*  <http://orcid.org/0000-0001-6319-6731>

## References

- A.C.E., U. S. 2010. HEC-RAS River Analysis System. *User's Manual, Version 4.1, November*, 1–790. <https://doi.org/CPD-68>.
- Akturk E, Altunel AO. 2019. Accuracy assesment of a low-cost UAV derived digital elevation model (DEM) in a highly broken and vegetated terrain. *Meas: J Int Meas Confederation*. 136(February 2019):382–386. doi:10.1016/j.measurement.2018.12.101.
- Annis A, Nardi F, Petroselli A, Apollonio C, Arcangeletti E, Tauro F, Belli C, Bianconi R, Grimaldi S. 2020. UAV-DEMs for small-scale flood hazard mapping. *Water*. 12(1717):1–16. doi:10.3390/w12061717.
- Aryal D, Wang L, Adhikari TR, Zhou J, Li X, Shrestha M, Wang Y, Chen D. 2020. A model-based flood hazard mapping on the southern slope of Himalaya. *Water*. 12(2). doi:10.3390/w12020540.
- Demir V, Kisi O. 2016. Flood Hazard Mapping by Using Geographic Information System and Hydraulic Model: Mert River, Samsun, Turkey. 2016.
- Farooq M, Shafique M, Khattak MS. 2019. Flood hazard assessment and mapping of River Swat using HEC-RAS 2D model and high-resolution 12-m TanDEM-X DEM (WorldDEM). *Natural Hazards*. 97(2):477–492. doi:10.1007/s11069-019-03638-9.
- Febriyanto A, Hidayah E, Halik G. 2018. Peak discharge estimation of Welang watershed in Pasuruan Regency. *Jurnal Rekayasa Sipil Dan Lingkungan*. 2(02):141. doi:10.19184/jrsl.v2i02.6906.
- Federal Geographical Data Committee. 1998. Geospatial positioning accuracy standards part 3: national standard for spatial data accuracy. *National Spatial Data Infrast*. 28. <http://www.fgdc.gov/standards/projects/FGDC-standards-projects/accuracy/part3/chapter3>.
- FGDC (Federal Geographic Data Committee). 1998. *Draft geospatial positioning accuracy standards. Part 2: standards for geodetic networks. FGDC-STD-007.2-1998*. 1–9. <https://www.fgdc.gov/standards/projects/FGDC-standards-projects/accuracy/part2/chapter2>.
- Horritt MS, Bates PD. 2002. Evaluation of 1D and 2D numerical models for predicting river flood inundation. *J Hydrol*. 268(1–4):87–99. doi:10.1016/S0022-1694(02)00121-X.
- IPCC. 2014. Climate change. *Proc Natl Acad Sci USA*. 111(SUPPL. 2):9340–9345. doi:10.1177/1368431015579968.
- Martínez-Carricondo P, Agüera-Vega F, Carvajal-Ramírez F, Mesas-Carrascosa FJ, García-Ferrer A, Pérez-Porrás FJ. 2018. Assessment of UAV-photogrammetric mapping accuracy based on variation of ground control points. *Int J Appl Earth Obs Geoinformation*. 72(May):1–10. doi:10.1016/j.jag.2018.05.015.
- Mourato S, Fernandez P, Pereira L, Moreira M. 2017. Improving a DSM obtained by unmanned aerial vehicles for flood modelling. *IOP Conference Series: Earth Environ Sci*. 95(2). doi:10.1088/1755-1315/95/2/022014.
- Muhadi NA, Abdullah AF, Bejo SK, Mahadi MR, Mijic A. 2020. The use of LiDAR-derived DEM in flood applications: a review. *Remote Sensing*. 12(14):1–20. doi:10.3390/rs12142308.
- Nardi F, Annis A, Baldassarre GD, Vivoni ER, Grimaldi S. 2019. GFPLAIN250m, a global high-resolution dataset of earth's floodplains. *Scientific Data*. 6(January):1–6. doi:10.1038/sdata.2018.309.
- Ongdas N, Akiyanova F, Karakulov Y, Muratbayeva A, Zinabdin N. 2020. Application of hec-ras (2d) for flood hazard maps generation for yesil (ishim) river in kazakhstan. *Water*. 12(10):1–20. doi:10.3390/w12102672.
- Peña F, Nardi F. 2018. Floodplain terrain analysis for coarse resolution 2D flood modeling. *Hydrology*. 5(4). doi:10.3390/hydrology5040052.
- Petroselli A, Vojtek M, Vojteková J. 2019. Flood mapping in small ungauged basins: a comparison of different approaches for two case studies in Slovakia. *Hydrol Res*. 50(1):379–392. doi:10.2166/nh.2018.040.
- Rizzi J, Gallina V, Torresan S, Critto A, Gana S, Marcomini A. 2016. Regional risk assessment addressing the impacts of climate change in the coastal area of the Gulf of Gabes (Tunisia). *Sustain Sci*. 11(3):455–476. doi:10.1007/s11625-015-0344-2.
- Sari P, Legono D, Sujono J. 2018. Performance of retarding basin in flood disaster risk mitigation in Welang River, East Java Province, Indonesia. *J Civil Eng Forum*. 4(2):109. doi:10.22146/jcef.31938.
- Shustikova I, Domeneghetti A, Neal JC, Bates P, Castellarin A. 2019. Comparing 2D capabilities of HEC-RAS and LISFLOOD-FP on complex topography. *Hydrol Sci J*. 64(14):1769–1782. doi:10.1080/02626667.2019.1671982.
- Sugiantara KB. 2020. *Pemodelan Hujan Aliran Dengan Metode Clark UH dan Snyder UH pada DAS Welang. Paper Report*, Unpublished.
- Vojtek M, Petroselli A, Vojteková J, Asgharinia S. 2019. Flood inundation mapping in small and ungauged basins: sensitivity analysis using the EBA4SUB and HEC-RAS modeling approach. *Hydrol Res*. 50(4):1002–1019. doi:10.2166/nh.2019.163.
- Vozinaki AEK, Morianou GG, Alexakis DD, Tsanis IK. 2017. Comparing 1D and combined 1D/2D hydraulic simulations using high-resolution topographic data: a case study of the Koiliaris basin, Greece. *Hydrological Sci J*. 62(4):642–656. doi:10.1080/02626667.2016.1255746.
- Yalcin E. 2019. Two-dimensional hydrodynamic modelling for urban flood risk assessment using unmanned aerial vehicle imagery: a case study of Kirsehir, Turkey. *J Flood Risk Manag*. 12(S1):1–14. doi:10.1111/jfr3.12499.